LIMNOLOGY
and
OCEANOGRAPHY: METHODS

ASLO

Limnol. Oceanogr.: Methods 19, 2021, 8–20

doi: 10.1002/lom3.10401

Surface elevation change evaluation in mangrove forests using a low-cost, rapid-scan terrestrial laser scanner

Ali Rouzbeh Kargar,[1]* **Richard A. MacKenzie,**[2] **Alexander Fafard,**[1] **Ken W. Krauss,**[3] **Jan van Aardt**[1]
[1]Chester F. Carlson Center for Imaging Science, Rochester Institute of Technology, Rochester, New York
[2]Forest Service, Institute of Pacific Islands Forestry, Hilo, Hawaii
[3]U.S. Geological Survey, Wetland and Aquatic Research Center, Lafayette, Louisiana

Mangrove forests have adapted to sea level rise (SLR) increases by maintaining their forest floor elevation via belowground root growth and surface sediment deposits. Researchers use surface elevation tables (SETs) to monitor surface elevation change (SEC) in mangrove forests, after which this information is used to assess SLR resiliency or to dictate active forest management for vulnerable systems. This method requires significant investments in terms of time and human resources and is limited in the number of points it can measure per plot. We use a low-cost, portable terrestrial laser scanning (TLS) system to assess SEC for three mangrove forests on Pohnpei Island (Federated States of Micronesia). Cloth simulation filtering was used for ground detection, after which results were refined by filtering points using angular orientation. Digital elevation models then were generated via kriging interpolation for data collected in 2017 and 2019, after which the heights of corresponding points were compared across years. Extreme elevation changes, due to disturbances such as footprints or fallen logs, were removed using interquartile range analysis. The TLS-obtained average SEC ranged between −6.92 and +6.01 mm, which exhibited an average consistency of 72% when compared to simultaneously collected SET data (root mean square error = 1.36 mm). We contend that this approach represents an improvement over the manual method, where very few points typically are used, that is, ≅ 36 points vs. ≅ 30,000 points in the case of TLS, and could contribute to improved monitoring and management of these rapidly changing forest environments.

Sea level rise (SLR) is one of the greatest threats that mangroves will face in the 21st century (Ward et al. 2016; Friess et al. 2019). Mangrove forests have kept up with or paced previous increases in SLR rates by maintaining their forest floor elevation. This is accomplished through root growth, sedimentation, resistance to soil compaction, and peat development (Krauss et al. 2014). Today, these processes are threatened by various human activities such as altered hydrology, sedimentation rates, or deforestation (Cahoon and Reed 1995; Krauss et al. 2010; Lang'at et al. 2014; Sasmito et al. 2016). As a result, efforts have increased to monitor surface elevation changes (SEC) in mangrove forests to develop more effective and robust conservation or restoration strategies on a global scale (Webb et al. 2013). For example, surface elevation of mangroves keeping up with or pacing SLR will result in forests that are more resilient to climate change and should be prioritized in overall conservation approaches such as implementation of no take zones or development of sustainable harvest practices (Krauss et al. 2010). Surface elevation of mangroves that are not keeping up well with SLR are more vulnerable to climate change and may require management actions such as the addition of sediments or out planting of mangrove trees (MacKenzie et al. 2016).

SEC is commonly measured in mangroves using surface elevation tables (SETs) or rod SETs (rSETs). SETs and rSETs are aluminum pipes or stainless-steel rods, respectively, driven through the mangrove sediment/peat to a point of refusal. The elevation of the forest floor is then measured relative to the top of the pipe/rod over time, typically at 9 points in 4 different directions from the pipe center for a total of 36 measurements per SET/rSET (Cahoon et al. 2002; Lynch et al. 2015). Once installed, each SET/rSET can provide a short-term (years to decades) assessment of whether the forest floor is building elevation or subsiding (Cahoon et al. 2002). This approach integrates aboveground processes occurring on the mangrove surface (sedimentation/accretion, erosion) with deeper belowground process such as root growth or peat collapse and provides an estimate of SEC at sub-cm resolutions (mm yr^{-1}). However, field-campaigns for collecting SET/rSET data are time consuming, labor intensive, and prone to human error as pins are manually set in presumably the same location at each time point. Furthermore, the number of points used for assessing the elevation change are relatively few, approximately

*Correspondence: axr7139@rit.edu

36 points per SET/rSET. All of these factors can result in a high standard error for the elevation change measurements using SET/rSETs. Error associated with repetitive SET/rSET remeasurement alone is 1.0–1.5 mm, and this can be compounded to 1.3–4.3 mm in wetland soils (Cahoon et al. 2002). The large standard error range decreases the reliability of the results obtained using the SET/rSET-based approach.

We propose an approach using a portable and rapid-scan terrestrial laser scanning (TLS) system (Compact Biomass Lidar [CBL]; Kelbe et al. 2015) to estimate SEC in mangrove forests. This approach is expected to be far more accurate than SET/rSETs, because it measures significantly more points (30,000–100,000) across a greater area of ~ 10 m radius (2–5 m radius plots, after data preprocessing) and reduced human bias or error as points are remeasured each time point via a laser return.

The application of TLS or CBL systems has increased rapidly in recent years for tasks including topographical surveys (e.g., Gallay et al. 2015), investigation of small-scale landslides (e.g., Wang et al. 2013), and collecting forest inventory measurements (e.g., Dassot et al. 2011; Kelbe et al. 2013; Rouzbeh Kargar et al. 2019). TLS are also being used more often to create high-resolution, small-scale (< 0.5 ha) digital elevation models (DEMs) for digital soil mapping (McBratney et al. 2003), natural hazard assessment (Arnone et al. 2016), and ecological species distribution studies (Guisan and Zimmermann 2000). The rapid growth in TLS use is due to the higher accuracy and detailed measurements that TLS can provide in forest systems with complex aboveground structures (e.g., mangroves) compared to airborne laser scanners (ALS) (McMahon et al. 2015; Baltensweiler et al. 2017). For example, Su and Bork (2006) reported an overestimation of 0.2 m in ALS-derived DEMs compared to TLS that was attributed to complexity in vegetation structure. Fan and Atkinson (2015) also found that areas with higher surface structural complexity introduce larger root mean square error (RMSE) values ($\sim$ 2–17 mm). These errors can be significantly reduced in close-range, fine-scale TLS scans. The trade-off with higher point densities and detailed measurements of TLS is that laser pulse scans can be obscured (reflected/absorbed) by obstacles, resulting in irregular point distribution and shadowing (occlusion) effects in the 3D point clouds that require more complex separation of ground and nonground returns compared to ALS data (Panholzer and Prokop 2013). Multiple TLS scans with different "viewsheds" are therefore typically required to form a single mega-point cloud to alleviate these concerns (Milan et al. 2007).

Another challenge when working with dense scans generated by TLS is detecting ground points. Current interpolation methods for detecting ALS ground points include minimum height filtering (Lee and Younan 2003), triangulated irregular network (TIN; Axelsson 2000), and cloth simulation filtering (CSF; Zhang et al. 2016). The interpolation (cell) resolution typically is based on point density and distribution, horizontal accuracy, and terrain complexity (Hengl 2006). For higher cell resolutions generated by TLS, the ground filtering method becomes more complex (Hseih et al. 2017), and the interpolation method used for generating the DEM from the detected TLS ground returns can impact the accuracy of the resulting elevation model. Of the different interpolation techniques used for DEM generation (e.g., linear interpolation, inverse distance weighting, kriging interpolation), kriging interpolation appears to be the most accurate (Oliver and Webster 1990; Meijering and Unser 2003). This is because kriging interpolation considers point weights that depend on the overall spatial arrangement of the points and, as a result, is more resilient to noise and typically produces more accurate DEMs, at the cost of increased processing requirements (Barbarella et al. 2017).

In this study, we compared the accuracy and effectiveness of a low-cost, rapid-scan TLS to standard SET measurements in quantifying SEC in three mangrove forests of Pohnpei Island in the Federated States of Micronesia. These forests are considered to be structurally complex with tertiary root and trunk structures (Krauss et al. 2003; Krauss et al. 2010). The CBL was used to generate DEMs in 2017 and 2019 at the same time periods that SETs were manually measured. CBL-generated DEMs and SET measurements were then compared between time points to quantify changes in the surface elevation of the forest floor with each respective method. In addition, the lidar (CBL) used in this study addresses the limitations of higher-cost scanners, for example, long scan time, power requirements, portability, and so on. The CBL generates rapid-scan (30 s per scan), but low-density data, due to higher angular step-width and lower pulse frequency, when compared to higher-cost, longer scan-time commercial scanners. The minimum angular step-width of CBL is 4.36 mrad (mrad), resulting in a lidar point cloud with lower associated point density when compared to higher cost systems, for which the minimum angular step width can be as small as 0.02 mrad (Kelbe et al. 2015). The minimum angular step width defines the angular (degree) intervals at which the scanner collects the data. As a result, our approach needs to be robust to issues caused by low-density data and complex structural environments. We hypothesize that by combining the lidar point clouds collected with different viewsheds in each plot and using a point filtering approach based on the angular orientation of the lidar points, we can evaluate the changes in mangrove forest floor elevation and increase the reliability and accuracy of the results compared to current SET/rSET methods.

Methods and materials

Study sites

Research was conducted in mangrove forests on the Western Pacific island of Pohnpei, one of the eastern most island states in the Federated States of Micronesia and in the Carolina island chain (6°50′59.99″N, 158°12′60.00″E). Pohnpei is a 35,000 ha, 782 m high volcanic island that receives large

amounts of unevenly distributed rainfall, ranging from 3500 to 5000 mm yr^{-1} (Krauss et al. 2003, 2007).

Mangrove forests represent approximately 16% of the land area of Pohnpei and can be divided into fringe, riverine, and interior hydrogeomorphic zones (Ewel et al. 1998*a*, 1998*b*). *Sonneratia alba* J. Smith, *Bruguiera gymnorrhiza* (L.) Lamk., and *Rhizophora apiculata* BL are commonly found in all zones (Krauss et al. 2010). Average stand heights range from 15 to 27 m, with trees in interior and riverine zones generally being taller than trees in fringe zones (Ewel et al. 2003).

Surface elevation tables

SETs were installed in 1998 in the Enipoas and Sapwalap mangrove forests to calculate SEC (Krauss et al. 2010). Aluminum pipes (7.6 cm in diameter) were driven into soil until refusal using a manual slammer, a notched, SET insert tube was attached to the top of the pipe and the entire aboveground portion of the SET was backfilled with cement. During each measurement, a portable SET table was attached to the insert tube. Nine fiberglass pins were then slid through nine holes in the SET table until they rested on top of the forest floor. The pin heights were then measured relative to the top of the SET table. The SET table was placed in four different directions relative to the aluminum pipe and releveled each time for a total of 36 measurements. Changes in the pin height relative to an initial starting point reflect the interaction of erosion, vertical accretion, soil expansion (from root growth), and shallow subsidence (Cahoon and Reed 1995; McKee et al. 2007). Three SETs were installed in the riverine, fringe, and interior zones of the Enipoas and Sapwalap mangrove forests for a total of 18 SETs, which were measured once a year from 1998 to 2004 and again from 2015 to 2019.

The CBL

In 2017 and 2019, we also scanned the surface elevation of eight 10-m-radius forest plots in Enipoas ($n = 1$) and Sapwalap ($n = 7$) using a low-cost, rapid-scan TLS (CBL; SICK LMS-151, SICK AG, Waldkirch, Germany) at low tide when the forest floor was completely exposed (see Fig. 1A). The low-cost CBL used for this project was built to address the limitations of higher-cost scanners in structural assessment of forest environments, such as low mobility and prolonged scan times (Van der Zande et al. 2006). The CBL allows rapid sampling of its surroundings, but this comes at the cost of its angular resolution and associated lidar point density being lower than typical higher-cost commercial systems (Kelbe et al. 2015). As a result, the algorithms developed for processing data need to be robust to issues caused by low-density lidar data. The CBL was mounted on a modified SET arm that allowed the CBL to be mounted to either SET or rSETs (Fig. 1B). Eight scans were collected in each plot, at 45° between-scan increments in a clockwise direction, with the starting point directed northward. The scans were collected with the CBL in a downward facing position to capture as many lidar ground returns as possible; this is counter to typical TLS use where the scanned lidar "hemisphere" is directed toward the upward-facing forests structures (Kelbe et al. 2013, 2015). The scanning scheme was consistent among all plots and no further adjustments were made, thereby minimizing data collection bias.

The scanner in the CBL (SICK LMS-151 unit, SICK AG, Waldkirch, Germany) uses a 905-nm laser pulsing at 27 kHz. The scanning mirror operates in a 270° plane. The scanner is attached to a rotation stage, rotating through 180°, enabling scanning of a 270° × 360° "hemisphere," though a 90° cone above the scanner remains unscanned. A maximum of two returns are digitized for each pulse. The specifications of CBL are presented in Table 1 (SICK AG Waldkirch: Nelson, 2009). Once the scans were complete, a photo in each cardinal direction (N, S, W, E) was also taken from each plot to help with interpretation of point clouds generated from the scans.

Lidar scan registration and downsampling

The first step in this work was to co-register the eight scans per plot using a combination of manual and automatic approaches. These point clouds cannot be registered accurately by automatic algorithms due to the complex structures of the scanned area. In our first step, we aligned two consecutively scanned or adjacent point clouds. This was done based on the structural tie points between the lidar point clouds using a pairwise registration technique, outputting a rigid transformation matrix (Zai et al. 2017). Afterward, we used the iterative closest point (ICP) algorithm to align the point clouds more accurately. The ICP finds the closest points between the two point clouds and determines the rotation and translation matrices, using the root mean square distance minimization approach (Besl and McKay 1992). It is important to mention that the first scan, which was directed northward, was considered as the reference point cloud, meaning that all other point clouds were registered in a manner as to be oriented northward. This was done to ensure that the generated DEMs are oriented similarly. After registering all the scans per plot for 2019 data, the resulting point clouds were aligned with those from 2017 in order to avoid any spatial and angular displacement between the detected ground points. This mismatch can occur if the scanner is not perfectly level in the adjacent scans, which realistically could occur given the difficult data collection conditions (mangrove root complexity, care required not to disturb sediment, etc.). In addition, based on the possible structural variation in the plots between the 2 years, for example, changes in forest floor elevation, and vegetation cover, there could be a spatial or angular displacement between the data collected in 2017 and 2019. We next downsampled the point clouds, since the areas closer to the scanner and directly at its nadir (0° zenith) are highly oversampled, due to the oversampling bias of the scanner in these regions, where the iterative mirror scans of the lidar crosses at the 0° zenith location as it rotates through 180°. The downsampling algorithm that we used is based on the spherical sampling scheme of the

Fig 1. (**a**) Interior site in the Enipoas mangrove forest that shows the structural complexity and aboveground roots typical of the forest plots we scanned and (**b**) the CBL scanner mounted on the modified SET arm and attached to the insert tube of the SET pipe. Photo credit: R. MacKenzie, USDA Forest Service.

TLS and considers higher weights for the points further from the scanner while assigning lower weights to points in closer proximity (Fafard et al. 2020). This approach maintains the structural attributes of the point cloud while effectively reducing oversampling and locational scan bias from our data.

Denoising the point cloud

Following the scan registration process, noise points in the data (i.e., outliers that do not relate to any structure in the lidar point cloud) were removed from the lidar point clouds. These outliers can affect the structural assessment accuracy and local point properties (e.g., point normal characteristics). We used the statistical outlier removal (SOR) algorithm (Rusu et al. 2008) for noise reduction. SOR is an algorithm which finds the mean distance of each point to all its neighboring points, and, with the assumption of a Gaussian distribution, the points with a mean distance outside a select threshold are labeled as outliers. This threshold is defined by the mean and standard deviation of the global distances between the points in the point cloud. The number of neighbors used for SOR analysis in this work was found by investigating the point density in manually detected structures, like stems, roots, and also some visible ground regions, that were located farther from the scanner but represented the geometric characteristics of these structures accurately. The number of neighbors for SOR assessment, which preserves these structures, was found to be five. Fig. 2 shows the point cloud for one of the plots after pre-processing (i.e., registration, downsampling, noise removal).

Table 1. Specifications of CBL instrumentation.

Range finder	Time of flight and intensity
Wavelength (nm)	905
Measured range (m)	5–20
Resolution (°)	0.25
Range accuracy (mm)	30
Scan duration (s)	33
Weight (kg)	3.9
Beam divergence (mrad)	15.0
Minimum angular step width (mrad)	4.36
Coverage (°)	270 × 360
Maximum pulse frequency (kHz)	27

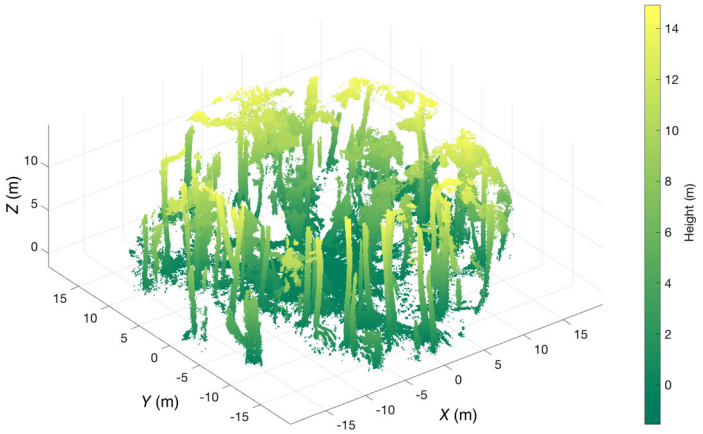

Fig 2. The height map of a point cloud after preprocessing from a single plot in the Sapwalap mangroves, including scan registration, downsampling, and noise removal. The structural complexity of these data can be seen in the point cloud, for example, aboveground roots.

Ground detection

Cloth simulation filtering

The points in the lidar point cloud had to be divided or classified into ground and nonground returns in order to generate a plot-level DEM. We used the CSF algorithm for ground detection (Zhang et al. 2016). We chose this method to limit the number of parameters needed to be set by the user, which can aid in generalizing this methodology for other environments. In this method, the point cloud is initially turned upside down, and then a 3D polynomial, known as "cloth," is fitted to the point cloud to detect the ground returns. The fit is evaluated by assessing the position of the cloth particles, which are constrained in a vertical direction. When a particle intersects with the lidar ground return, it is set as unmovable. Finally, the relative position of the particles is assessed by external and internal forces in the cloth to detect anomalies (e.g., a steep slope between two adjacent points or extreme elevation changes) (Zhang et al. 2016). This process yields the first output for refinement to accurately detect ground lidar returns.

Angle-based filtering of ground returns

Conventional ground detection algorithms do not typically provide very accurate ground returns, mainly due to the structural complexity and increased shadowing (occlusion) effects in TLS data. Additional postprocessing steps, like removing the aboveground points based on structural metrics, therefore may be required in order to generate accurate results using these algorithms on TLS data. We visually identified root points that were classified as ground in the plots where the aboveground roots had segments very close to the ground and/or were horizontally oriented, even after applying CSF and extracting ground returns. Next, we filtered the detected ground returns based on their angular orientation in order to remove these erroneous points (Fig. 3). This was done by extracting the facets of the point cloud (Dewez et al. 2016), which are planes fit to the points of the 3D point cloud. The FACTES plugin in CloudCompare software (Version 2.9.1) was used in this step. This plugin applies the Kd-Tree and Fast Marching algorithm to extract the facets (Bentley 1975; Sethian 1996). Kd-Tree is a method for segmenting the data by grouping points in k-dimensional space, and Fast Marching is a numerical technique for determining the associated boundary values. Both of these approaches segment the lidar point cloud into subsets, find the planar surfaces, and generate polygons from them. We found that the angular orientation of these points ranges between 12° and 23° by manually investigating the angular distribution of the roots close to the ground in eight plots. We can detect the true ground returns, with low errors of commission, by filtering out the roots (Fig. 3).

Interpolating the ground points and generating DEMs

We wanted to ensure that DEM interpolation was based upon areas within that scanned plot that had adequate TLS point densities and did not include areas that had low point returns or highly variable lidar point densities. We therefore limited our scanned plots to only include areas where the density of ground points was significantly higher, in terms of the range of two standard deviations from the mean of the ground lidar point density of the entire scanned plot, and performed interpolation only in this area of each plot. In the areas of low point density, the resultant DEM quality could be highly affected by the interpolation as low point densities in complex topography decrease the accuracy of elevation mapping in those regions. The resulting radii of interpolation ranged between 1.8 and 3.1 m among the various plots. The detected ground points then were interpolated to generate a DEM for each plot. We used the kriging interpolation technique in this study; kriging is a method of interpolation in which the interpolated values are modeled by a Gaussian process (Trochu 1993). Kriging predicts the value of a function at a given point by computing a weighted average of the values in the neighboring cells. It presumes that the distance between the points represents spatial correlation. Kriging uses semivariogram analysis to determine the value for each location, where the semivariance is calculated by measuring the dispersion of all observations that fall below the mean or target value of a set of data (Matheron 1963). As a result, in kriging, the weights depend on the overall spatial arrangement of the measured points, resulting in more robustness to noise points and outliers. We interpolated the ground returns to 1×1 cm (x, y) grid resolution (Fig. 4).

Assessing the surface elevation change

Elevation change assessment using nearest neighbor search

A linear nearest neighbor search (NNS) technique was applied to the 2D grid of X and Y coordinates from the two DEMs (Zlot and Bosse 2009) in order to compare the exact same points from 2017 and 2019 data. NNS finds the point in a set which is closest to a specified input point. This closeness is typically evaluated via a dissimilarity function; the more similar the objects, the smaller the function values (Knuth 1973). Finally, the elevation (Z values) of the corresponding points of the two DEMs were subtracted to identify locations where either an elevation gain or loss has occurred between 2017 and 2019 and its associated value (Fig. 5). However, some extreme points were obtained during this elevation change assessment process. These points were found to be either a result of human interaction (i.e., foot prints) or fallen logs. This information was acquired by studying the scanned plots from images, observations of the field crew, or examination of photos that were also collected. In these cases, the lidar can either consider the top of the log as the ground return, resulting in an extreme elevation gain, or after the log is removed, an extreme elevation loss will be recorded by the scanner. This can be reconciled against

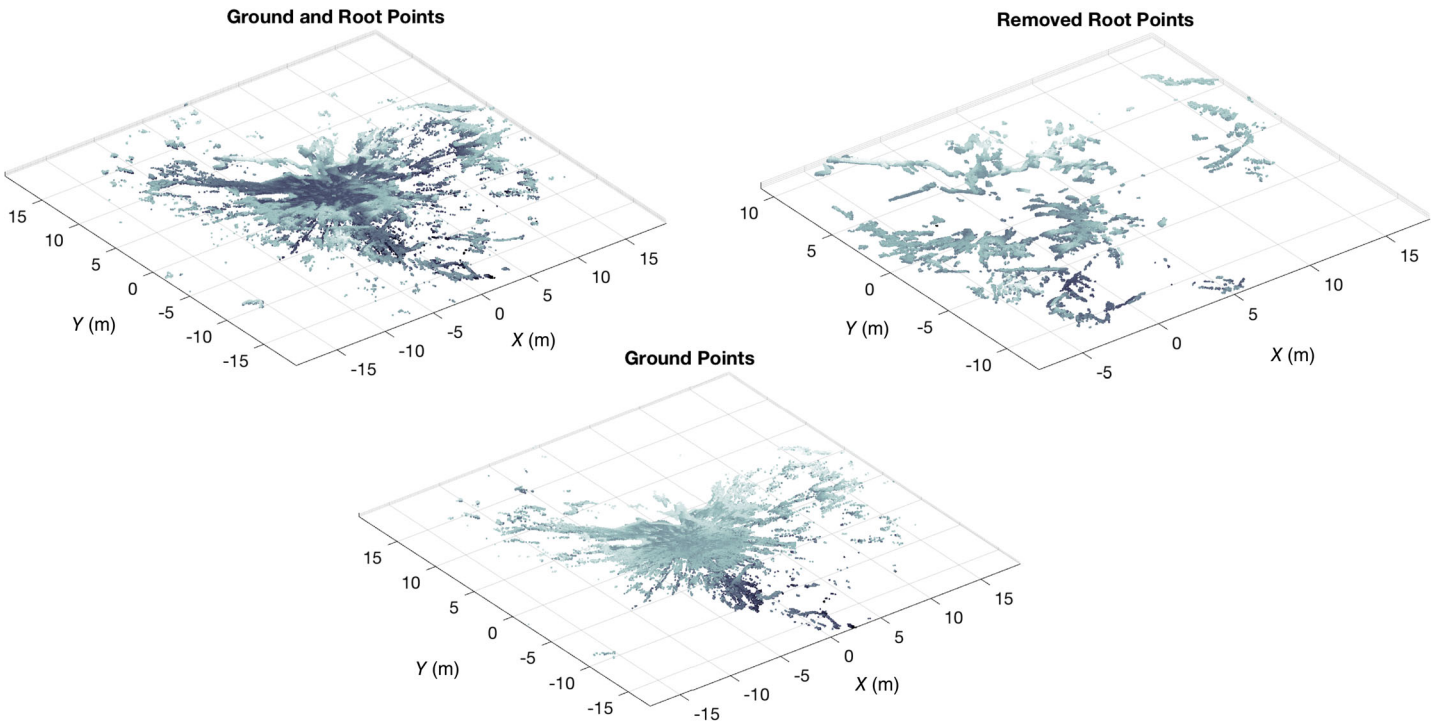

Fig 3. The removal of incorrectly classified root points by filtering the facets of the point cloud using their angular orientation.

standard SET rules for determining the soil surface in specific mangrove wetlands (Lynch et al. 2015).

Removal of extreme elevation changes

The points with extreme elevation change described above were removed using interquartile range (IQR) analysis. IQR is the difference between the first and third quartiles (*Q*1 and *Q*3), or the medians of the lower and upper half of the data, respectively (Wright 1996). Points that were further than $2 \times \text{IQR}$ from the median of the data (*Q*2 or second quartile) were labeled as outliers. This wide range was chosen for

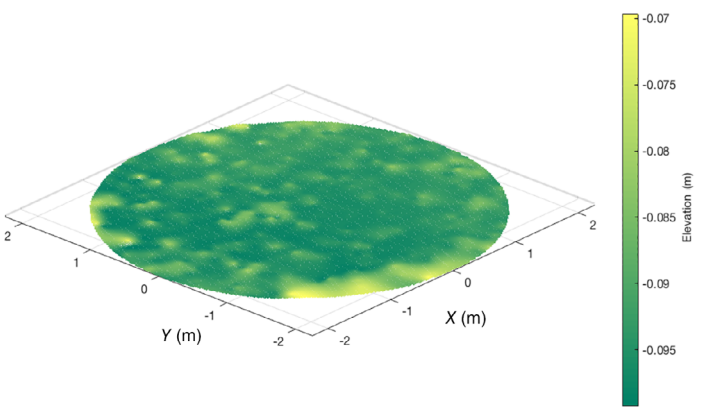

Fig 4. An elevation "heat map" of a DEM generated for the Enipoas Riverine C plot from 2019 data. This DEM was created for a 2-m radius plot, due to the higher density of ground points within this area.

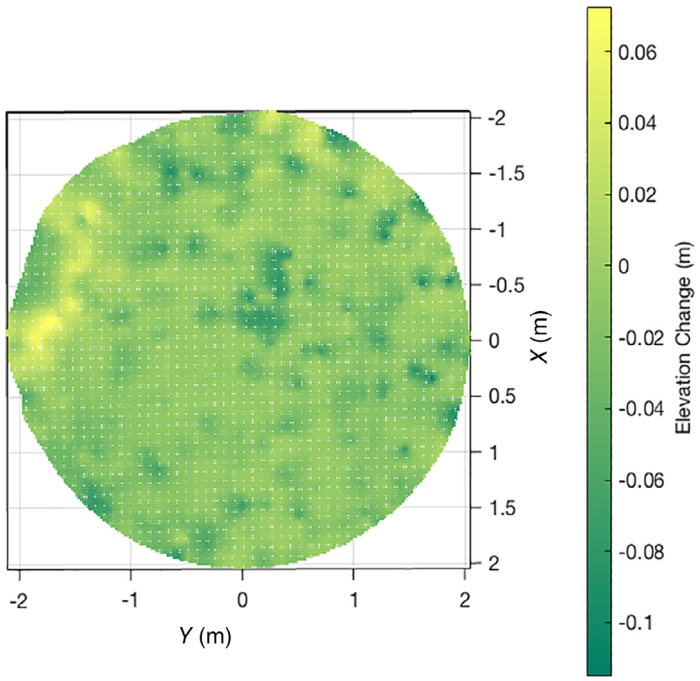

Fig 5. The height map of the elevation changes between the DEMs generated from the 2017 and 2019 data from Sapwalap Fringe B. The negative values show elevation loss from 2017 to 2019, and the positive values represent elevation gain. It can be seen that there are extreme elevation changes in this DEM, which after studying the site, was found to be related to recently fallen logs in this plot.

interquartile analysis, since only extreme elevation changes were flagged for removal. The average of the elevation change in each plot was then determined, and the consistency was assessed by comparing the lidar-derived SEC with the field-measured elevation data, collected by SETs.

Results

The SEC was assessed in eight plots using the TLS point clouds and then compared to field-measured forest floor elevation changes based on the SET approach (Fig. 6; Table 2). Surface elevation change determined from CBL scans were typically within 1 mm (0.2–1.1 mm) of the SET measurements. The only exceptions were Sapwalap Riverine A (4.3 mm) and C (2.2 mm) and Sapwalap Interior B (2.6 mm). This was due to elevation changes measured with the CBL that were not captured by the 36 SET pin measurements (i.e., Fig. 5). Standard error from CBL surface elevation measurement was also 10–70× lower than SET-based elevation change measurements.

The consistency metric used in this study was found using the following equation:

$$\text{Consistency} = \frac{\text{Field value} - |\,\text{Field value} - \text{Lidar value}\,|}{\text{Field value}},$$

where Lidar value is the average of elevation change found by the TLS in each plot, and the Field value is the average elevation change collected by the SETs in that plot. It is worth noting here that a coordinate-based, point-to-point comparison between the TLS and SET approaches would have been more ideal; however, the traditional SET-based approach does not record the within-plot coordinate of each reading. Even if one could determine the exact *x*,*y* coordinates of the pins, there may not be an exact lidar hit at that point, especially across years, which would be needed for a direct comparison. The SET/rSET-based approach yields a plot-level assessment of elevation change, which could be construed as a significant benefit of the TLS-based approach, that is, that researchers/practitioners are provided with spatially explicit, within-plot elevation change data driven by the large number of points analyzed using the TLS vs. only 36 SET points. The calculated consistency ranged between 56% and 92%, with an average of 72%, and an RMSE of 1.36 mm. The consistency was affected by the complexity of the scene, like root structures, which affect the ground detection accuracy. The consistency was lower in plots where the roots' structures contained higher complexity closer to the ground, which decreased the accuracy of ground detection. As the accuracy of ground detection decreases, interpolation introduces more error. These errors could not be avoided due to the very complex structure of these mangrove forests and the confusion caused by factors

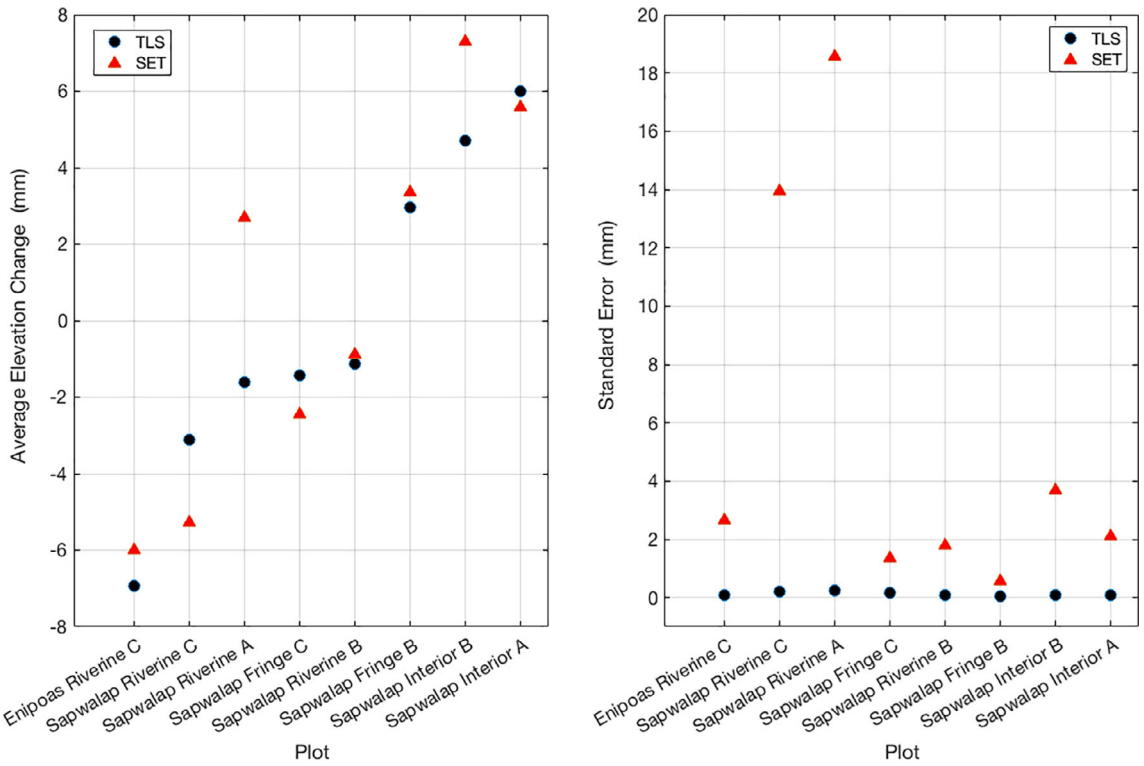

Fig 6. Per plot average elevation change and standard error obtained using TLS and SET. It can be seen that the standard error is lower for the TLS compared to the SET in all the measured plots.

Table 2. Per plot average elevation change acquired by TLS- and SET-based methods.

Plot name	Dominant species	Method	Average elevation change (mm)	Standard error (mm)
Enipoas Riverine C	*Bruguiera gymnorrhiza* (64%)	TLS	−6.92	0.08
	Rhizophora apiculata (33%)	SET	−6.0	2.64
Sapwalap Fringe B	*R. apiculata* (60%)	TLS	2.97	0.06
		SET	3.36	0.57
Sapwalap Fringe C	*R. apiculata* (60%)	TLS	−1.44	0.15
		SET	−2.45	1.33
Sapwalap Riverine A	*R. apiculata* (67%)	TLS	−1.62	0.25
		SET	2.68	18.55
Sapwalap Riverine B	*R. apiculata* (67%)	TLS	−1.14	0.10
		SET	−0.90	1.78
Sapwalap Riverine C	*R. apiculata* (67%)	TLS	−3.10	0.22
		SET	−5.29	13.94
Sapwalap Interior A	*R. apiculata* (60%)	TLS	6.01	0.08
		SET	5.59	2.11
Sapwalap Interior B	*R. apiculata* (60%)	TLS	4.72	0.10
		SET	7.28	3.66

like human interaction, for example, footsteps, and fallen logs in the studied plots.

Table 2 shows that there was an average increase in the RMSE of 0.06 mm in the plots where *R. apiculata* is the dominant species. This increase in RMSE was attributed to the higher structural complexity of these species, thereby making the ground detection results less accurate.

Discussion

The methodology presented in this study significantly decreases the labor and time requirements of SEC data collection using CBL (minutes vs. hours) compared to more traditional SET/rSETs used around the world (Webb et al. 2013). CBL also appears to increase the accuracy of SEC measurements by measuring a greater number of points within the forest plots and also reduces human error associated with SET measurements. For example, the SET method uses 36 points per plot for SEC measurement, all of which are assessed by lowering the pins down until they are resting on the forest floor surface. This approach introduces significant bias and error, in terms of when exactly an operator deems the SET pins to have made full contact with the underlying surface or if the operator pushes the pins into the sediment. The TLS-based approach, on the other hand, is completely automated (unbiased) in its 3D scanning operation and yields upwards of 30,000 elevation points per plot. This can increase the repeatability and reliability of the presented approach when compared to SET. This also results in significantly lower error (Table 2).

The use of CBL for SEC measurements also significantly expands localized SET plot measurements to a larger plot-level scan radius, DEMs' radius values ranging from 1.8 to 3.1 m, only restricted by the lidar scanner engineering specifications. This allows the CBL to capture changes in elevation that the SET pins can miss. This was evident by the large differences we observed between SEC measurements made in Sapwalap Riverine A and C and Sapwalap Interior C.

Although potentially more efficient, there are drawbacks using TLS to assess the SEC in mangrove forests. The main drawback is that TLS measurements can only be performed when the forest floor is exposed (e.g., low tide, after significant rainfall events); since the 905-nm laser of the TLS used in this work cannot penetrate the water, the submerged ground surface cannot be detected. Future efforts should include using lidar systems with the laser in a wavelength range which can penetrate water, so that the measurements can be done throughout the year. However, one should consider the impact of the system wavelength on the power returned to the lidar sensor from objects such as vegetation cover, roots, and stems.

The novel use of a low-density TLS to assess SEC in structurally complex mangrove forests proved to be an effective and efficient method. Previous studies also were successful in evaluating land surface dynamics using TLS data. Bodin et al. (2008) evaluated changes in the structure of rock glaciers via assessment of internal deformation of ice and debris mixtures using high point density TLS data, approximately 2500 points per second. The sub-decimeter resolution of the scanner used by Bodin et al. (2008), in theory, leads to increases in the accuracy of derived DEMs. On the other hand, the lower-density data acquired by CBL, at millimeter resolution, introduces challenges to ground detection and associated assessment of mangrove forest structure and elevation changes, while decreasing the cost and time of data collection. Additional steps therefore are needed alongside the typical

ground detection techniques, in order to address this issue. In this work, we presented an angle-based lidar point filtering approach to improve the ground detection and elevation change assessment. The performance of this approach deteriorates when the complexity of the aboveground root structures increases, especially when these roots are located in close proximity to the ground and oriented horizontally, which introduces confusion in ground detection algorithms. Su and Bork (2006) studied the effect of vegetation density and structure on DEM accuracy and found that where the structural attributes of the vegetation were more complex, for example, the slope gradient of the vegetation components were either steep or variable, the accuracy of DEM decreases. They observed a maximum overestimation of 0.2 m in the lidar-derived DEMs, where the vegetation exhibited higher structural complexity. In another study, Fan and Atkinson (2015) found that the RMSE value for DEM accuracy assessment is highly dependent on the surface complexity. They found RMSE values in the range of approximately 2–17 mm. The areas with more complex surface structural attributes, roughness in the case of their study, provided the highest RMSE value, while smoother surfaces were associated with the lower RMSE values. The aboveground mangrove roots caused the same problem in our data, and the angle-based filtering was used to address this issue.

In a more recent work, Stovall et al. (2019) evaluated the ability of a TLS to detect the hummocks in black ash wetlands in Northern Minnesota. They used the slope analysis of the TLS points for detecting the hummocks, similar to what was done in our work to filter the root points, and acquired good results (91% accuracy) in retaining the hummocks by thresholding the surface model elevation and slope. The authors rasterized the ground-classified points and did not interpolate empty cells, and regardless, acquired smooth surface models. This was attributed to the specifications of the TLS they used, the Faro Focus 120 3D phase-shift TLS, and also the structural attributes of the study site. The Faro Focus 120 3D phase-shift TLS provides much denser data when compared to the CBL, being able to collect up to 976,000 points per scan (Castro et al., 2018), while the CBL collects up to approximately 300,000 points per scan in natural environments. In addition, the beam divergence in the Faro Focus 120 3D is 0.19 mrad, which provides a higher resolution compared to the 15-mrad beam divergence of the CBL, while the range accuracy for the Faro Focus 120 3D is as low as 2 mm (at ranges < 120 m), while the range accuracy for the CBL is specified as 30 mm (at ranges < 50 m) (Kelbe et al. 2015). The Faro Focus 120 3D therefore in effect yields a denser lidar point cloud and enables more accurate structural assessment of the targets. However, as mentioned earlier, the low-cost CBL system boasts a reduction in both collection time, that is, based on a scan duration of 33 s for the CBL compared to a few minutes for Faro Focus 120, and cost of data acquisition (Faro Laser Scanner Focus 3D Manual, Lake Mary, Florida 2013). Furthermore, the study site in our work (i.e., mangrove forests) theoretically introduces additional structural complexity when compared to black ash wetlands. The aboveground roots in mangrove forests make the detection of aboveground structures and also ground detection more challenging, while the black ash forests do not contain any aboveground structures, other than vegetation and tree stems. Another confounding factor is that Stovall et al. (2019) logically planned their TLS campaign to coincide with the period when the vegetation cover was minimal (leaf-off for deciduous trees) and when there was the least likelihood of aboveground water. This in effect reduces forest structural complexity, and as a result makes it difficult to generalize such a method to other forest environments, such as mangroves. Although the detection of hummocks and mangrove roots seem to be similar problems, hummocks exhibit higher elevation differences relative to the bare ground points, when compared to mangrove roots that are located close to the ground, and confuse the ground detection algorithm. The angular orientation of the hummocks also is much different when compared to the lower mangrove roots; hummocks are mostly vertically oriented and as a result can be detected via slope analysis of the surface model. Near-ground mangrove root sections with a horizontal orientation (12°–23°), on the other hand, make ground vs. nonground lidar point classification significantly more challenging. Finally, we opted for a robust interpolation approach, that is, kriging interpolation, to increase the accuracy of surface model and minimize the impact of mangrove root occlusion effects. Although the interpolation approach from Stovall et al. (2019) resulted in a smooth surface model, we were required to boost the robustness of our approach, given the lower point density generated by the CBL scanner, albeit at the trade-off benefits of mobility, scan time, and instrument cost.

The DEM generation and evaluation approach presented in this work also can be used in areas where mangrove tree densities are even higher, unlike the more traditional ALS implementations where canopy cover can adversely affect the performance of the ground detection algorithms (Spaete et al. 2011). Spaete et al. (2011) studied the impact of vegetation and canopy cover on lidar-derived DEMs and found that tree species with steep stem/branching angles and higher canopy density resulted in higher RMSE values for DEM accuracy assessment (0.220 m). Low-angle and low-density canopy species, for example, low sagebrush, on the other hand, yielded lower RMSE values for DEM evaluation (0.072 m). In other studies, vegetation-related errors of up to 1 m have been reported when the ALS DEM data were used to model structural attributes of forest environments, for example, coastal saltmarsh areas (Rosso et al. 2006) and scrubland areas (Palamara et al. 2007). We encountered similar problems when we tested out the effectiveness of the CBL to measure elevation change Distichilis dominated salt marsh systems in the Chesapeake Bay (Kargar, unpubl. data).

It is important to note that such a TLS-based method can also improve satellite-based forest ecosystem assessments, specifically by aiding calibration of airborne and spaceborne remote sensing data. As an example, Alsaaideh et al. (2013) used Landsat Enhanced Thematic Mapper plus (ETM+) and coincident DEMs to detect mangroves in six islands, located in southern Japan. Although they reported high classification accuracies (89.3%–93.6%), they mentioned that improvements in DEM accuracy can improve the results of mangrove detection via satellite imagery. In another study, Takaku et al. (2004) evaluated the DEMs acquired by the Panchromatic Remote Sensing Instrument for Stereo Mapping (PRISM), carried on the Advanced Land Observing Satellite. The authors assessed the accuracy of DEMs for various land covers, for example, an urban area, paddy field, forest area, and a truck farm. The results show that the RMSE values for the forest area is higher than for other land covers, 5.204 m and < 5.0 m, respectively. The higher RMSE in the forest area was attributed to lidar occlusion effects, which made the detection of height edges challenging. An approach like the one presented in our work, for which the DEM accuracy RMSE values are on the millimeter order, can be used to calibrate DEMs generated using satellite and airborne data, and to increase the accuracy and reliability of those models. In addition, mangroves contain complex aboveground root structures which affect the performance of ground detection, while in a less complex forest environment, the accuracy of DEM assessment likely will increase. One important consideration in our approach is related to our objective to generalize the approach for any potential mangrove plot, regardless of the species composition and plot-specific structural attributes. It is of course expected that more complex root structures, that is, frequency and density of roots closer to the ground, may result in a decrease in ground detection accuracy. However, our aim was to develop a unified approach for mangrove plots, without the need to parameterize models for factors like species, root variability, and so on, thereby generalizing this approach when working with low-density 3D point cloud data, even when species classification may be challenging. For example, information on the dominant species in each of the plots is listed in Table 2. *R. apiculata* arguably has the highest level of structural complexity, that is, more dense and complex root shapes. An average increase of 0.06 mm in the standard error values in *R. apiculata*-dominant plots was attributed to the higher structural complexity of this species. A future improvement may involve incorporating relevant species-specific parameters into 3D algorithms and building upon the method we have developed in this study. Future work can also include an increase in the number of plots to improve the statistical validity of the results and an improvement in the ground detection accuracy by incorporating more structural metrics of the lidar point clouds during ground filtering, other than the angular orientation of the lidar points used in this work.

Conclusions

We presented an approach to assess SEC in mangrove forests, which are regarded as forest environments with complex root structures, using a low-cost, portable, and rapid-scan TLS system. The complex aboveground root mass in mangroves can introduce errors to ground detection algorithms and subsequently decrease the accuracy of SEC assessment. We reduced the impacts of occlusion effects and low-density data by registering eight scans in each plot. We used the angular orientation of facets/points for filtering ground from non-ground lidar returns during preprocessing in order to improve the accuracy of ground detection, which can be used in environments where the structural complexity of the data introduces challenges to existing ground detection techniques. We evaluated the changes in DEM elevation between two sets of data, from 2017 and 2019, to estimate the elevation changes in these mangrove forests. We observed a 72% consistency between the traditional SET-based and the novel TLS-based approaches, while the latter approach exhibited a significantly lower standard error range. However, the structural complexity of the plot, for example, low-lying and horizontally oriented aboveground roots, can introduce challenges and impact the performance of this approach. We concluded that the TLS can address issues associated with SET/rSETs such as a limited number of observed elevation locations per plot and operator objectivity and can provide more accurate and consistent estimation of forest floor dynamics. This approach can lead to a more accurate/precise assessment of SEC that can be used to identify mangroves that are more resilient or vulnerable to increased rates of SLR. This information can then be used to help develop and guide more effective management for mangrove forests and the many ecosystem services that they provide. A potential improvement in the accuracy and precision of SEC assessments in mangrove forests will also likely contribute to enhanced, better calibrated satellite-based forest information products and enhance our ability to monitor the impact of climate change on global mangrove ecosystems. Future work should incorporate improved ground filtering approaches, by using additional structural parameters other than the angular orientation method used in this work, and also extend this approach to structural assessment in other forest environments.

References

Alsaaideh, B., s A. Al-Hanbali, R. Tateishi, T. Kobayashi, and N. T. Hoan. 2013. Mangrove forests mapping in the southern part of Japan using Landsat ETM+ with DEM. J. Geogr. Inf. Syst. **5**: 369–377. doi:10.4236/jgis.2013.54035.

Arnone, E., A. Francipane, A. Scarbaci, C. Puglisi, and L. V. Noto. 2016. Effect of raster resolution and polygon-conversion algorithm on landslide susceptibility mapping.

Environ. Model. Softw. **84**: 467–481. doi:10.1016/j.envsoft.2016.07.016.

Axelsson, P. 2000. DEM generation from laser scanner data using adaptive TIN models. Int. Arch. Photogram. Remote Sens. **33**: 110–117.

Baltensweiler, A., L. Walthert, C. Ginzler, F. Sutter, R. S. Purves, and M. Hanewinkel. 2017. Terrestrial laser scanning improves digital elevation models and topsoil pH modelling in regions with complex topography and dense vegetation. Environ. Model. Softw. **95**: 13–21. doi:10.1016/j.envsoft.2017.05.009.

Barbarella, M., M. Fiani, and A. Lugli. 2017. Uncertainty in terrestrial laser scanner surveys of landslides. Remote Sens. **9**: 113. doi:10.3390/rs9020113.

Bentley, J. L. 1975. Multidimensional binary search trees used for associative searching. Commun. ACM **18**: 509–517. doi:10.1145/361002.361007.

Besl, P. J., and N. D. McKay. 1992. Method for registration of 3-D shapes, p. 586–607. *In* Sensor fusion IV: Control paradigms and data structures, v. **1611**. International Society for Optics and Photonics. doi:10.1109/34.121791.

Bodin, X., P. Schoeneich, and S. Jaillet. 2008. High-resolution DEM extraction from terrestrial LiDAR topometry and surface kinematics of the creeping alpine permafrost: The Laurichard rock glacier case study (Southern French Alps). Institute of Northern Engineering, University of Alaska at Fairbanks **1**: 137–142.

Cahoon, D. R., J. C. Lynch, B. C. Perez, B. Segura, R. D. Holland, C. Stelly, G. Stephenson, and P. Hensel. 2002. High-precision measurements of wetland sediment elevation: II. The rod surface elevation table. J. Sediment. Res. **72**: 734–739. doi:10.1306/020702720734.

Cahoon, D. R., and D. J. Reed. 1995. Relationships among marsh surface topography, hydroperiod, and soil accretion in a deteriorating Louisiana salt marsh. J. Coast. Res.: 357–369.

Castro, R. A., Dourado, M. N., Almeida, J. R. D., Lacava, P. T., Nave, A., Melo, I. S. D., Quecine, M. C. 2018. Mangrove endophyte promotes reforestation tree (Acacia polyphylla) growth. brazilian journal of microbiology. **49**(1): 59–66. doi:10.1016/j.bjm.2017.04.002.

Dassot, M., T. Constant, and M. Fournier. 2011. The use of terrestrial LiDAR technology in forest science: Application fields, benefits and challenges. Ann. Forest Sci. **68**: 959–974. doi:10.1007/s13595-011-0102-2.

Dewez, T. J., D. Girardeau-Montaut, C. Allanic, and J. Rohmer. 2016. Facets: A cloudcompare plugin to extract geological planes from unstructured 3D point clouds. Int. Arch. Photogram. Remote Sens. Spatial Inf. Sci. **41**. doi:10.5194/isprsarchives-XLI-B5-799-2016.

Ewel, K. C., J. A. Bourgeois, and T. G. Cole. 1998a. Variation in environmental characterisitics and vegetation in high-rainfall mangrove forests, Kosrae, Micronesia. Global Ecol. Biogeogr. Lett. **7**: 49–56. doi:10.1111/j.1466-8238.1998.00267.x.

Ewel, K. C., R. D. Hauff, and T. G. Cole. 2003. Analyzing mangrove forest structure and species distribution on a Pacific Island. Phytocoenologia **33**: 251–266. doi:10.1127/0340-269X/2003/0033-0251.

Ewel, K. C., S. Zheng, Z. S. Pinzon, and J. A. Bourgeois. 1998b. Environmental effects of canopy gap formation in high-rainfall mangrove forests. Biotropica **30**: 510–518. doi:10.1111/j.1744-7429.1998.tb00091.x.

Fafard, A., A. Rouzbeh Kargar, and J. van Aardt. 2020. Reducing terrestrial lidar sampling bias—weighted spherical sampling of point clouds. IEEE Geosci. Remote Sens. Lett.

Fan, L., and P. M. Atkinson. 2015. Accuracy of digital elevation models derived from terrestrial laser scanning data. IEEE Geosci. Remote Sens. Lett. **12**: 1923–1927. doi:10.1109/LGRS.2015.2438394.

Faro Laser Scanner Focus 3D Manual (2013). Lake Mary (FL).

Friess, D. A., K. Rogers, C. E. Lovelock, K. W. Krauss, S. E. Hamilton, S. Y. Lee, R. Lucas, J. Primavera, A. Rajkaran, and S. Shi. 2019. The state of the world's mangrove forests: Past, present, and future. Annu. Rev. Environ. Resour. **44**: 89–115. doi:10.1146/annurev-environ-101718-033302.

Gallay, M., J. Ka□uk, Z. Hochmuth, J. D. Meneely, J. Hofierka, and V. Sedlák. 2015. Large-scale and high-resolution 3-D cave mapping by terrestrial laser scanning: A case study of the Domica Cave, Slovakia. Int. J. Speleol. **44**: 6. doi:10.5038/1827-806X.44.3.6.

Guisan, A., and N. E. Zimmermann. 2000. Predictive habitat distribution models in ecology. Ecol. Model. **135**: 147–186. doi:10.1016/S0304-3800(00)00354-9.

Hengl, T. 2006. Finding the right pixel size. Comput. Geosci. **32**: 1283–1298.

Hseih, B. C., S. Khawam, N. Ioannis, M. Muir, K. Le, H. Siddiqui, and S. F. Yeh. 2017. A 3D stacked programmable image processing engine in a 40 nm logic process with a detector array in a 45 nm CMOS image sensor technologies, p. 4–7. *In* Proceedings of the 2017 International Image Sensor Workshop, Hiroshima, Japan.

Kelbe, D., P. Romanczyk, J. van Aardt, and K. Cawse-Nicholson. 2013. Reconstruction of 3D tree stem models from low-cost terrestrial laser scanner data, p. 873106. *In* Laser radar technology and applications XVIII, v. **8731**. International Society for Optics and Photonics.

Kelbe, D., J. van Aardt, P. Romanczyk, M. van Leeuwen, and K. Cawse-Nicholson. 2015. Single-scan stem reconstruction using low-resolution terrestrial laser scanner data. IEEE J. Select. Topic. Appl. Earth Observ. Remote Sens. **8**: 3414–3427.

Knuth, D. E. 1973. The art of computer programming, vol. 3: Searching and sorting. Reading (MA): Addison-Wisley.

Krauss, K. W., J. A. Allen, and D. R. Cahoon. 2003. Differential rates of vertical accretion and elevation change among aerial root types in Micronesian mangrove forests. Estuarine Coast. Mar. Sci. **56**: 251–259.

Krauss, K. W., D. R. Cahoon, J. A. Allen, K. C. Ewel, J. C. Lynch, and N. Cormier. 2010. Surface elevation change and

susceptibility of different mangrove zones to sea-level rise on Pacific high islands of Micronesia. Ecosystems **13**: 129–143.

Krauss, K. W., B. D. Keeland, J. A. Allen, K. C. Ewel, and D. J. Johnson. 2007. Effects of season, rainfall, and hydrogeomorphic setting on mangrove tree growth in Micronesia. Biotropica **39**: 161–170.

Krauss, K. W., K. L. McKee, C. E. Lovelock, D. R. Cahoon, N. Saintilan, R. Reef, and L. Chen. 2014. How mangrove forests adjust to rising sea level. New Phytol. **202**: 19–34.

Lang'at, J. K. S., J. G. Kairo, M. Mecuccini, S. Bouillon, M. W. Skov, S. Waldron, and M. Huxham. 2014. Rapid losses of surface elevation following tree girdling and cutting in tropical mangroves. PLoS One **9**: e107868. doi:10.1371/journal.pone.0107868

Lee, H. S., and N. H. Younan. 2003. DTM extraction of LiDAR returns via adaptive processing. IEEE Trans. Geosci. Remote Sens. **41**: 2063–2069. doi:10.1109/TGRS.2003.813849.

Lynch, J. C., P. Hensel, and D. R. Cahoon. 2015. The surface elevation table and marker horizon technique: A protocol for monitoring wetland elevation dynamics. National Park Service. doi:10.13140/RG.2.1.5171.9761.

MacKenzie, R. A., P. B. Foulk, J. V. Klump, K. Weckerly, J. Purbospito, D. Murdiyarso, D. C. Donato, and V. N. Nam. 2016. Sedimentation and belowground carbon accumulation rates in mangrove forests that differ in diversity and land use: A tale of two mangroves. Wetlands Ecol. Manage. **24**: 245–261. doi:10.1007/s11273-016-9481-3.

Matheron, G. 1963. Principles of geostatistics. Econ. Geol. **58**: 1246–1266. doi:10.2113/gsecongeo.58.8.1246.

McBratney, A. B., M. M. Santos, and B. Minasny. 2003. On digital soil mapping. Geoderma **117**: 3–52. doi:10.1016/S0016-7061(03)00223-4.

McKee, K. L., D. R. Cahoon, and I. C. Feller. 2007. Caribbean mangroves adjust to rising sea level through biotic controls on change in soil elevation. Global Ecol. Biogeogr. **16**: 545–556. doi:10.1111/j.1466-8238.2007.00317.x.

McMahon, S. M., D. P. Bebber, N. Butt, M. Crockatt, K. Kirby, G. G. Parker, and E. M. Slade. 2015. Ground based LiDAR demonstrates the legacy of management history to canopy structure and composition across a fragmented temperate woodland. Forest Ecol. Manage. **335**: 255–260. doi:10.1016/j.foreco.2014.08.039.

Meijering, E., and M. Unser. 2003. A note on cubic convolution interpolation. IEEE Trans. Image Process. **12**: 477–479. doi:10.1109/TIP.2003.811493.

Milan, D. J., G. L. Heritage, and D. Hetherington. 2007. Application of a 3D laser scanner in the assessment of erosion and deposition volumes and channel change in a proglacial river. Earth Surf. Process. Landforms J. Br. Geomorphol. Res. Group **32**: 1657–1674. doi:10.1002/esp.1592.

Nelson A., Reuter H. I., Gessler P. 2009. DEM production methods and sources. Developments in soil science. **33**: 65–85.

Oliver, M. A., and R. Webster. 1990. Kriging: A method of interpolation for geographical information systems. Int. J. Geogr. Inf. Syst. **4**: 313–332. doi:10.1080/02693799008941549.

Palamara, D. R., M. Nicholson, P. Flentje, E. Baafi, and G. M. Brassington. 2007. An evaluation of airborne laser scan data for coalmine subsidence mapping. Int. J. Remote Sens. **28**: 3181–3203. doi:10.1080/01431160600993439.

Panholzer, H., and A. Prokop. 2013. Wedge-filtering of geomorphologic terrestrial laser scan data. Sensors **13**: 2579–2594. doi:10.3390/s130202579.

Rosso, P. H., S. L. Ustin, and A. Hastings. 2006. Use of lidar to study changes associated with Spartina invasion in San Francisco Bay marshes. Remote Sens. Environ. **100**: 295–306. doi:10.1016/j.rse.2005.10.012.

Rouzbeh Kargar, A., R. MacKenzie, G. P. Asner, and J. Van Aardt. 2019. A density-based approach for leaf area index assessment in a complex forest environment using a terrestrial laser scanner. Remote Sens. **11**: 1791. doi:10.3390/rs11151791.

Rusu, R. B., Z. C. Marton, N. Blodow, M. Dolha, and M. Beetz. 2008. Towards 3D point cloud based object maps for household environments. Robot. Autonom. Syst. **56**: 927–941. doi:10.1016/j.robot.2008.08.005.

Sasmito, S. D., D. Murdiyarso, D. A. Friess, and S. Kurnianto. 2016. Can mangroves keep pace with contemporary sea level rise? A global data review. Wetlands Ecol. Manage. **24**: 263–278. doi:10.1007/s11273-015-9466-7.

Sethian, J. A. 1996. A fast marching level set method for monotonically advancing fronts. Proc. Nat. Acad. Sci. **93**: 1591–1595. doi:10.1073/pnas.93.4.1591.

SICK. 2009. LMS100/111/120/151 laser measurement systems operating instructions. Reute, Germany: SICK AG Waldkirch.

Spaete, L. P., N. F. Glenn, D. R. Derryberry, T. T. Sankey, J. J. Mitchell, and S. P. Hardegree. 2011. Vegetation and slope effects on accuracy of a LiDAR-derived DEM in the sagebrush steppe. Remote Sens. Lett. **2**: 317–326. doi:10.1080/01431161.2010.515267.

Stovall, A., J. Diamond, R. Slesak, D. McLaughlin, and H. Shugart. 2019. Quantifying wetland microtopography with terrestrial laser scanning. Remote Sens. Environ. **232**: 111271. doi:10.1016/j.rse.2019.111271.

Su, J., and E. Bork. 2006. Influence of vegetation, slope, and lidar sampling angle on DEM accuracy. Photogram. Eng. Remote Sens. **72**: 1265–1274. doi:10.14358/PERS.72.11.1265.

Takaku, J., N. Futamura, T. Iijima, T. Tadono, M. Shimada, and R. Shibasaki. 2004, September. High resolution DEM generation from ALOS PRISM data-simulation and evaluation, p. 4548–4551. *In* IGARSS 2004. 2004 IEEE International Geoscience and Remote Sensing Symposium, v. **7**. IEEE. doi:10.1109/IGARSS.2004.1370166.

Trochu, F. 1993. A contouring program based on dual kriging interpolation. Eng. Comput. **9**: 160–177. doi:10.1007/BF01206346.

Van der Zande, D., W. Hoet, I. Jonckheere, J. van Aardt, and P. Coppin. 2006. Influence of measurement set-up of ground-based LiDAR for derivation of tree structure. Agricult. Forest Meteorol. **141**: 147–160. doi:10.1016/j.agrformet.2006.09.007.

Wang, L. J., K. Sawada, and S. Moriguchi. 2013. Landslide susceptibility analysis with logistic regression model based on FCM sampling strategy. Comput. Geosci. **57**: 81–92. doi:10.1016/j.cageo.2013.04.006.

Ward, R. D., D. A. Friess, R. H. Day, and R. A. MacKenzie. 2016. Impacts of climate change on mangrove ecosystems: A regional overview. Environ. Health Sustain. **2**: 1–25.

Webb, E. L., D. A. Friess, K. W. Krauss, D. R. Cahoon, G. R. Guntenspergen, and J. Phelps. 2013. A global standard for monitoring coastal wetland vulnerability to accelerated sea-level rise. Nat. Climate Change **3**: 458–465. doi:10.1038/nclimate1756.

Wright, D. B. 1996. Understanding statistics: An introduction for the social sciences. Sage.

Zai, D., J. Li, Y. Guo, M. Cheng, P. Huang, X. Cao, and C. Wang. 2017. Pairwise registration of TLS point clouds using covariance descriptors and a non-cooperative game. ISPRS J. Photogram. Remote Sens. **134**: 15–29. doi:10.1016/j.isprsjprs.2017.10.001.

Zhang, W., J. Qi, P. Wan, H. Wang, D. Xie, X. Wang, and G. Yan. 2016. An easy-to-use airborne LiDAR data filtering method based on cloth simulation. Remote Sens. **8**: 501. doi:10.3390/rs8060501.

Zlot, R., and M. Bosse. 2009. Place recognition using keypoint similarities in 2D lidar maps, p. 363–372. *In* Experimental robotics. Berlin, Heidelberg: Springer.

Acknowledgments

We thank Ethan Hughes, Eugene Eperiam, and Emos Eperiam for assistance in data collection. Any use of trade, product, or firm names is for descriptive purposes only and does not imply endorsement by the U.S. Government. This research was funded by United States Forest Service, Pacific Southwest Research Station.

Conflict of interest

The authors declare no conflict of interest.

Submitted 07 November 2019
Revised 02 June 2020
Accepted 29 September 2020

Associate editor: Ivona Cetinic